An Enhanced *In Vivo* Stable Isotope Labeling by Amino Acids in Cell Culture (SILAC) Model for Quantification of Drug Metabolism Enzymes*[S]

A. Kenneth MacLeod‡, Padraic G. Fallon§, Sheila Sharp‡, Colin J. Henderson‡, C. Roland Wolf‡, and Jeffrey T.-J. Huang‡¶

Many of the enzymes involved in xenobiotic metabolism are maintained at a low basal level and are only synthesized in response to activation of upstream sensor/effector proteins. This induction can have implications in a variety of contexts, particularly during the study of the pharmacokinetics, pharmacodynamics, and drug–drug interaction profile of a candidate therapeutic compound. Previously, we combined *in vivo* SILAC material with a targeted high resolution single ion monitoring (tHR/SIM) LC-MS/MS approach for quantification of 197 peptide pairs, representing 51 drug metabolism enzymes (DME), in mouse liver. However, as important enzymes (for example, cytochromes P450 (Cyp) of the 1a and 2b subfamilies) are maintained at low or undetectable levels in the liver of unstimulated metabolically labeled mice, quantification of these proteins was unreliable. In the present study, we induced DME expression in labeled mice through synchronous ligand-mediated activation of multiple upstream nuclear receptors, thereby enhancing signals for proteins including Cyps 1a, 2a, 2b, 2c, and 3a. With this enhancement, 115 unique, lysine-containing, Cyp-derived peptides were detected in the liver of a single animal, as opposed to 56 in a pooled sample from three uninduced animals. A total of 386 peptide pairs were quantified by tHR/SIM, representing 68 Phase I, 30 Phase II, and eight control proteins. This method was employed to quantify changes in DME expression in the hepatic cytochrome P450 reductase null (HRN) mouse. We observed compensatory induction of several enzymes, including Cyps 2b10, 2c29, 2c37, 2c54, 2c55, 2e1, 3a11, and 3a13, carboxylesterase (Ces) 2a, and glutathione S-transferases (Gst) m2 and m3, along with down-regulation of hydroxysteroid dehydrogenases (Hsd) 11b1 and 17b6. Using DME-enhanced *in vivo* SILAC material with tHR/SIM, therefore, permits the robust analysis of multiple DME of importance to xenobiotic metabolism, with improved utility for the study of drug pharmacokinetics, pharmacodynamics, and of chemically treated and genetically modified mouse models. ***Molecular & Cellular Proteomics 14: 10.1074/mcp.M114.043661, 750–760, 2015.***

Metabolism is listed as the primary clearance mechanism for approximately three quarters of prescribed drugs (1). Of this metabolism, three quarters is carried out by enzymes of the CYP superfamily (1). The US Food and Drug Administration and European Medicines Agency recommend the assessment of metabolism by CYP1A2, CYP2B6, CYP2C8, CYP2C9, CYP2C19, CYP2D6, and CYP3A as early as possible during the preclinical development of a novel therapeutic agent (2, 3). As the expression of most of these CYP isoforms (and of other DMEs (drug metabolizing enzymes)[1] and transporters) can be induced in response to chemical challenge, with potential implications for the pharmacokinetic and phar-

From the ‡Jacqui Wood Cancer Centre, Medical Research Institute, Ninewells Hospital and Medical School, University of Dundee, Dundee DD1 9SY, Scotland; §School of Medicine, Trinity Biomedical Sciences Institute, Trinity College Dublin, Dublin 2, Ireland

⌘ *Author's Choice*—Final version full access.

Received, August 8, 2014 and in revised form, December 22, 2014

Published, MCP Papers in Press, January 5, 2015, DOI 10.1074/mcp.M114.043661

Author contributions: A.K.M. and J.T.H. designed research; A.K.M., S.S., C.J.H., and J.T.H. performed research; P.G.F. contributed new reagents or analytic tools; A.K.M., S.S., C.R.W., and J.T.H. analyzed data; A.K.M., P.G.F., C.J.H., C.R.W., and J.T.H. wrote the paper.

[1] The abbreviations used are: DME, drug metabolizing enzyme; ADH/Adh, alcohol dehydrogenase; AHR/Ahr, aryl hydrocarbon receptor; AKR/Akr, aldo-keto reductase; ALDH/Aldh, aldehyde dehydrogenase; AQUA, absolute quantification; Arnt, aryl hydrocarbon receptor nuclear translocator; CAR/Car, constitutive androstane receptor; CBR/Cbr, carbonyl reductase; CES/Ces, carboxylesterase; COMT/Comt, catechol o-methyltransferase; CYP/Cyp cytochrome P450; DDI, drug–drug interaction; EPHX/Ephx, epoxide hydrolase; FDR, false discovery rate; FMO/Fmo, flavin-containing monooxygenase; GST/Gst, glutathione s-transferase; HRN, hepatic reductase null; HSD/Hsd, hydroxysteroid dehydrogenase; Mgst, microsomal glutathione s-transferase; MRM, multiple reaction monitoring; PK, pharmacokinetic; PD, pharmacodynamics; Por, cytochrome P450 reductase; PXR/Pxr, pregnane x receptor; RDH/Rdh, retinol dehydrogenase; Rxr, retinoid x receptor; SEM, standard error of the mean; SD, standard deviation; SILAC, stable isotope labeling by amino acids in cell culture; SULT/Sult, sulfotransferase; tHR/SIM, targeted high resolution single ion monitoring; UDP, uridine diphosphate; UGT/Ugt, uridine diphosphate-glucuronosyltransferase.

macodynamic properties of both the agent being administered, and of other drugs (drug–drug interaction), it is therefore also recommended that the capacity of the candidate agent to induce DME expression be assessed at an early stage (2, 3).

The majority of clinically relevant drug-mediated CYP induction is known to occur through activation of two closely related nuclear receptors; the pregnane x receptor (PXR) and the constitutive androstane receptor (CAR). These receptors are highly promiscuous, mediating the induction of multiple Phase I and Phase II enzymes in response to diverse exogenous and endogenous stimuli (4–8). Their activity is assessed through measurement of the levels of specific downstream targets, primarily CYP3A and CYP2B6 (2, 3). A third receptor, the aryl hydrocarbon receptor (AHR) is less promiscuous, with a target battery more distinct from those of PXR and CAR (4, 8), but is a central mediator of CYP1A induction, and its activity can be inferred from the levels of these enzymes (2, 3). An alternative approach to the direct measurement of CYP protein is assay of metabolic conversion of specific probe substrates (*e.g.* 1-hydroxylation of midazolam for CYP3A), often in the presence or absence of specific inhibitors (*e.g.* ketoconazole) or inducers (*e.g.* rifampicin). This approach is of utility *in vivo*, but is limited to the small number of CYP for which these specific agents are available and is not generally applicable to other DMEs, although efforts to identify probes specific for members of the UDP glucuronosyltransferase (UGT) subfamily have met with some success (9, 10).

Aside from CYP, most of the remaining Phase I reactions are carried out by alcohol dehydrogenase (ADH), aldehyde dehydrogenase (ALDH), aldo-keto reductase (AKR), carbonyl reductase (CBR), epoxide hydrolase (EPHX), esterase (*e.g.* CES), flavin-containing monooxygenase (FMO), and hydroxysteroid/retinoid dehydrogenase (HSD/RDH) superfamilies (1, 11). Subsequent Phase II (conjugation) reactions are carried out by enzymes including UGT, GST, sulfotransferase (SULT), and methyltransferase (*e.g.* COMT) (1, 11). In the context of drug development, greater emphasis is being placed on understanding non-CYP mediated interactions, such as with FMO, ADH, and ALDH, but particularly with UGT (2). Currently, the US Food and Drug Administration recommends assessment of the interaction with UGTs 1A1, 1A3, 1A4, 1A6, 1A9, 2B7, and 2B15 (2).

Because of the unavailability of specific probe substrates, DME levels are usually assessed by Western blotting and microarray/RT-PCR. However, concerns relating to the cross-reactivity of antibodies within highly homologous protein subfamilies, and to the potential discordance between mRNA and protein levels (12), have led to a growing interest in the development of LC-MS/MS based methodology for the quantification of DMEs (13–18) and drug transporters (19–22) in various species. Among these techniques, the most common is multiple reaction monitoring (MRM)-based absolute quantification (AQUA) (23). The main drawback of this approach is the inability to control the recovery of peptides during sample processing steps prior to the addition of stable isotope peptide(s), potentially leading to quantification inaccuracies. Such bias can be severe when in-gel or filter-assisted protocols are followed (24). In order to circumvent this problem, we have previously developed a DME-targeted *in vivo* SILAC-based method wherein 197 peptide pairs, representing 51 DMEs, were quantified in a single sample (two LC-MS/MS analyses) (25). The workflow followed the principles of stable isotope dilution LC-MS commonly employed in the analytical laboratory for small molecule analysis, with *in vivo* SILAC material ($^{13}C_6$-lysine-labeled liver lysate) used as an internal standard to control recovery and ionization efficiencies. The ratio(s) of light to heavy peptides in defined retention time and m/z window(s) were used to quantify protein expression. This method served to circumvent the uncertainties generated during sample preparation in AQUA, as both light and heavy analytes share near-identical chemical properties, environment, and processing. The number of peptides measured, and hence the confidence of protein quantification, was greater than in a typical AQUA analysis. Furthermore, stress tests such as dilution linearity enabled the removal of peptides with poor analytical performance, providing a high level of consistency and reproducibility (25). It was, however, noted that this workflow omitted key Cyps because of their low level of constitutive expression in the heavy internal standard liver. The objective of the current study was, therefore, to generate a metabolically labeled mouse model which would allow direct quantification of as many DME, both inducible and basally expressed, of relevance to xenobiotic metabolism as possible. This "DME-enhanced" *in vivo* SILAC model was characterized in detail and its utility was demonstrated in the proteomic characterization of the compensatory effects that occur following the deletion of P450 reductase in the hepatocyte specific P450 reductase null (HRN) mouse (26).

EXPERIMENTAL PROCEDURES

Reagents—5-Pregnen-3β-ol-20-one-16α-carbonitrile (PCN), phenobarbital (PB), β-naphthoflavone (βNF), rifampicin (RIF), 1,4-Bis-[2-(3,5-dichloropyridyloxy)]benzene,3,32,5,52-tetrachloro-1,4-bis-(pyridyloxy)benzene (TCPOBOP), ethoxyquin (EQ), corn oil (CO), DL-dithiothreitol (DTT), and iodoacetamide (IAA) were purchased from Sigma (Dorset, UK). 2,3,7,8-tetrachloro-p-dioxin (TCDD) was purchased from Toronto Research Chemicals (Toronto, Canada). Trypsin Gold was purchased from Promega (Madison, WI).

Animal Husbandry and Dosing—All unlabeled mice were maintained under standard animal house conditions, with free access to food and water, and a 12-h light/12-h dark cycle. All animal work was carried out on male 8-week-old C57BL/6J mice in accordance with the Animal Scientific Procedures Act (1986) and after local ethical review. Mice were administered compounds (or corresponding vehicle) in a final volume of 10 μl/g of body weight as detailed in supplemental Table S1. In the case of PCN/PB/βNF mixture dosing, PCN and βNF were suspended in corn oil at 2x concentration and PB was dissolved in PBS at 2x concentration. Each preparation was then administered at 5 μl/g of body weight, with a 15 min interval to allow

dispersal of the first solution. After sacrifice, liver tissue was excised and snap-frozen in liquid nitrogen for storage at −80 °C.

SILAC Animals—SILAC labeled C57BL/6J mice were generated by feeding $^{13}C_6$ Lysine diet (Silantes GmbH, Munich, Germany) over four generations, as described (27). Adult female mice were on SILAC diet for 20 days before males were added for generation of F1 offspring. F1 female offspring were maintained on SILAC diet and bred for F2 labeled pups. This was repeated for four generations. F5 male and female mice were maintained on SILAC diet and used when 6–8 weeks of age. Animals were housed in a specific pathogen-free facility in individually ventilated and filtered cages under positive pressure. All animal experiments were performed in compliance with the Irish Medicines Board regulations and approved by the Trinity College Dublin's BioResources ethical review board.

Sample Preparation—For LC-MS/MS, frozen liver tissue was thawed in nine volumes of SDT lysis buffer (4% SDS, 0.1 M DTT, and 100 mM Tris-HCl, pH7.6) then homogenized by rotor-stator (2 × 5 s at 20 k revolutions). The homogenate was heated for 5 min at 95 °C then briefly sonicated (2 × 5 s). Debris was pelleted by centrifugation at 16,000 × *g* for 10 min. The supernatant containing protein for analysis was removed, aliquoted, and stored at −80 °C until use. Protein samples were separated by SDS-PAGE on a 12% bis-tris gel analysis in MOPS running buffer supplemented with antioxidant (Invitrogen, Paisley, UK). A total of 30 and 20 μg protein was loaded into each well for 10 and three fraction analysis, respectively. Gels were stained with Coomassie blue R250, destained, then rehydrated. Each gel lane was cut into two bands (Band 1: 80–40 kDa, Band 2: 40–0 kDa), with a clean scalpel. These were sliced finely (ca. 1 × 1 mm cubes) and collected in 1.5 ml protein LoBind Eppendorf tubes (Eppendorf, Hamburg, Germany). In-gel trypsin-mediated protein digest and extraction of peptides was carried out according to the method of Shevchenko and colleagues (28). Peptide sample concentration was determined by measurement of A280 on a Nanodrop spectrophotometer (Thermo Fisher Scientific, Waltham, MA) and adjusted to 0.2 mg/ml in water containing 0.1% (v/v) trifluoroacetic acid and 2% (v/v) acetonitrile. For Western blotting, microsomal and cytosolic fraction were prepared and analyzed as described previously (29, 30). Briefly, liver tissue was homogenized in three volumes KCl buffer (1.15% w/v potassium chloride and 10 mM potassium phosphate, pH7.4) by rotor-stator (2 × 5 s at 20k revolutions). The homogenate was centrifuged at 11,000 × *g* for 15 min to pellet debris and the supernatant was ultracentrifuged at 100,000 × *g* for 1 h. The supernatant (cytosolic fraction) was retained, whereas the resulting pellet (microsomal fraction) was resuspended in KCl buffer containing 0.25 M sucrose. Protein concentration was determined by Bradford assay and adjusted to 1 mg/ml in LDS sample buffer (Invitrogen). Samples were separated by electrophoresis through 10% acrylamide gels for 1 h at 200 V, then transferred onto nitrocellulose membranes for 1 h at 100 V. Antibodies for Cyp detection have been summarized previously (31). Antibodies for Gst were a kind gift from Professor John Hayes, University of Dundee (32). Rabbit anti-GAPDH was purchased from Sigma (product number G9545).

Liquid Chromatography and Mass Spectrometry—A nanoflow liquid chromatograph (Agilent 1200, Agilent, Santa Clara, CA) with a LTQ-Orbitrap XL (Thermo Fisher Scientific) was used to analyze the protein digests. Approximately 0.4 μg total peptide was loaded onto a trap column at a flow rate of 10 μl/min for 3 min and the flow was then reversed to an Agilent Zorbex nano C18 column (0.0075 mm ID; 15 cm; 3 μm particle size). The peptides were resolved with a 3 h binary gradient at a flow rate of 300 nL/min as follows: 0% Buffer B for 5 min followed by 2–30% Buffer B for 140 min, 30–90% Buffer B for 15 min, 90–0% Buffer B for 10 min, and 0% Buffer B for 10 min. Buffer A contained 2% acetonitrile and 0.1% formic acid in water and Buffer B contained 0.1% formic acid in acetonitrile. The column was periodically cleaned with a 2 μl injection of buffer containing 50% acetonitrile and 0.1% formic acid in water. A Proxeon nanospray source with a stainless steel emitter (Thermo Fisher Scientific) was used to interface the Agilent nanoLC and LTQ-Orbitrap. Spray voltage was set at 1.8kV. The Orbitrap was tuned using Glu-Fibrinogen B peptide. For the protein/peptide identification, a method that consisted of full scans between 330–1500 a.m.u (in Orbitrap) and data dependent MS/MS with top six precursor ions (2^+ to 4^+ charged) in LTQ was employed. Orbitrap was operated in a profile mode at the resolution of 30,000 or 60,000 with a lock mass set at 445.1200 (polycyclodimethylsiloxane (33)), LTQ was operated in a centroid mode with isolation width = 1 (*m/z*), normalized collision energy = 0.25, and activation time = 30 ms. The max fill time for Orbitrap and LTQ were set at 500 ms and 50 ms, respectively. A dynamic exclusion of 30 s was used to maximize the acquisition of MS2 on peptides with lower intensity. For tHR/SIM analysis, a method that consisted of full scans between 330–1500 a.m.u (in Orbitrap) and data dependent MS/MS scans with or without defined precursors was employed. A dynamic exclusion of 30 s and a threshold of 500 counts to trigger MS2 were also applied for MS/MS scans. Nontargeted data dependent MS/MS was performed when there was no targeted precursor found in the MS scan. Further details can be found in the method and tune files submitted to PRIDE as supplemental Files S1 and S2.

Data Analysis—Protein and peptide database search was carried out using PEAKS version 6 (Bioinformatics Solutions, Waterloo, Canada) with the UniprotKB mus musculus (taxid: 10090) reference proteome set (43,238 entries, downloaded 25.02.14). The precursor mass tolerance was set at 7 ppm and fragment ion mass tolerance set at 0.5 amu. Cysteine carbamidomethylation was selected as a fixed modification. SILAC lysine K6 was selected as a fixed modification when metabolically labeled tissue was under study. Methionine was selected as a variable modification. A maximum of two miscleavages were allowed. Quantification of the predefined targeted peptides was carried out using SIEVE version 2.0 (Thermo Fisher Scientific) using two seed files, depending on the molecular weight region of the gel being analyzed, containing retention time and *m/z* information. The precursor mass tolerance was set to 5 ppm and the minimal intensity for alignment was set automatically, with intensities derived from the first monoisotopic peak. Data from SIEVE were exported to Excel 2010 (Microsoft, Redmond, WA) for calculation of light to heavy peptide ratios. Before each light/heavy comparison, a baseline correction was applied. This involved the subtraction of the percentage of light signal that originated from the metabolically labeled liver, as determined through analysis of the heavy lysate alone in SIEVE with the full seed files. This enabled correction for the effect of incomplete labeling of protein in the internal standard. The average subtraction was ~2% (*i.e.* an average of 98% labeling efficiency). For protein quantification, light to heavy protein ratios were calculated within samples by summing average intensity values for all light peptides for each protein, then dividing by the corresponding heavy value. Light to heavy protein ratios within each sample were then normalized individually by adjustment of the median value to one. Biological replicates were normalized to the average of control before calculation of fold changes. During manual curation of SIEVE output from the HRN analysis, nine peptide pairs were removed because of incorrect charge state assignation by the software. For calculation of statistical significance, normalized values were log2-transformed then analyzed by unpaired *t* test with Holm-Šidák correction for multiple comparisons (Alpha = 0.05) using Prism 6 (Graphpad, La Jolla, CA).

RESULTS

Concept of Pathway-Enhanced In Vivo SILAC—A schematic concept of pathway-enhanced *in vivo* SILAC in com-

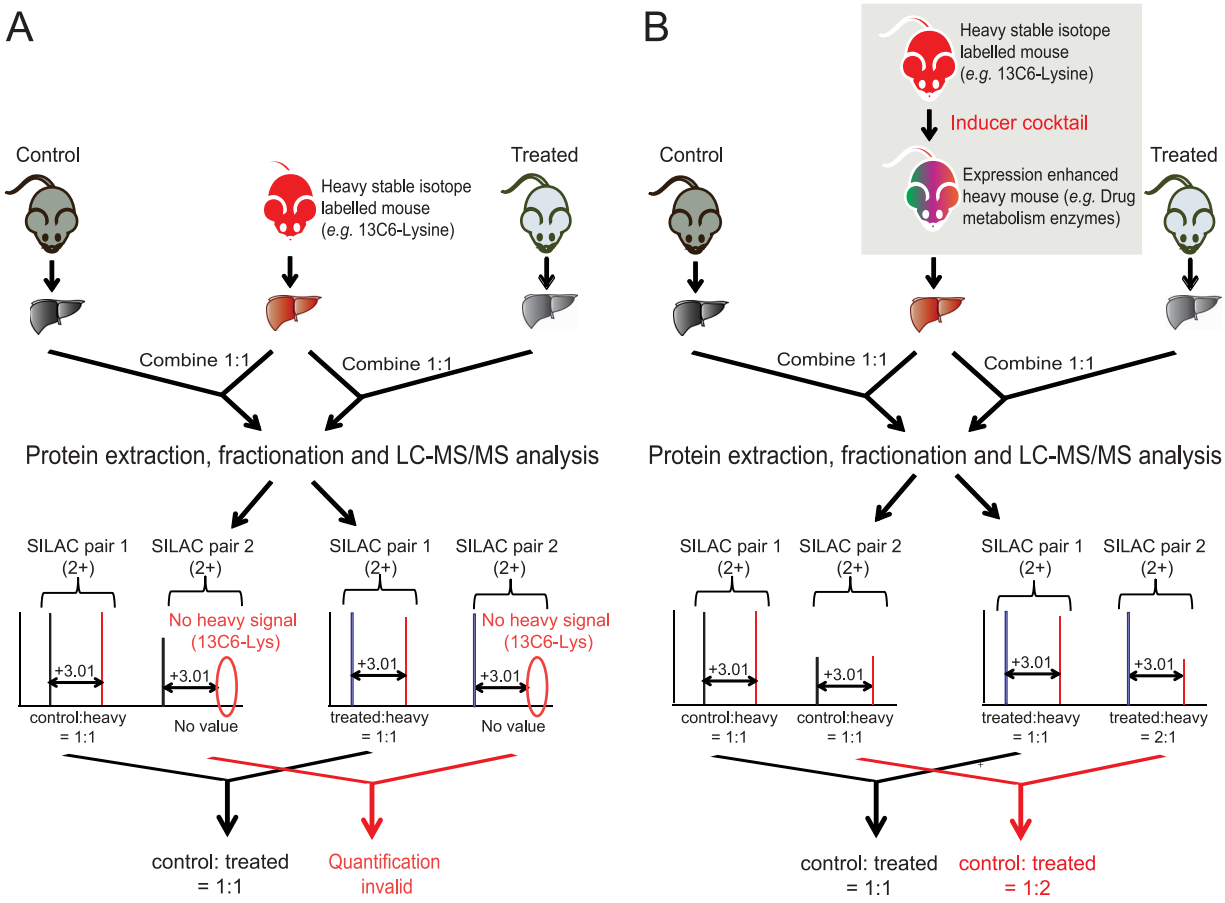

FIG. 1. **Pathway-enhanced *in vivo* SILAC.** *A*, A typical "spike-in" *in vivo* SILAC workflow. Metabolically labeled mouse liver tissue lysate is combined 1:1 with experimental samples (control and treated), followed by protein extraction, fractionation and LC-MS/MS analysis. When both light and heavy peptide species are present, fold changes can be compared between experimental samples (SILAC pair 1). When the heavy species is absent, a comparison is not feasible (SILAC pair 2). *B*, Targeted induction of proteins of interest in the metabolically labeled mouse circumvents this problem.

parison to conventional *in vivo* SILAC is shown in Fig. 1. In a typical "spike-in" workflow, metabolically labeled mouse liver tissue lysate is combined 1:1 with liver lysates from experimental samples, followed by protein extraction, fractionation, and LC-MS/MS analysis. Light to heavy ratios from monoisotopic peaks are calculated for each peptide of interest in individual samples, with fold changes across samples calculated using the ratio: ratio value (*e.g.* SILAC pair 1, Fig. 1*A*). In instances where light peptide signals from the experimental animals are detected but the corresponding heavy peptide from the spiked-in lysate is not present, the comparison of these two samples using typical SILAC is impossible (SILAC pair 2, Fig. 1*A*). By dosing the metabolically labeled mouse with compound(s) selected to elicit a specific response, which culminates in up-regulation of the protein(s) of interest prior to tissue harvest, this problem can be resolved (Fig. 1*B*).

Identification of a DME Inducer Mixture—In order to effect a widespread induction of DME expression in mouse liver, we attempted to identify a combination of chemicals that would activate Pxr, Car, and Ahr simultaneously (Fig. 2*A*). In isolation, the Pxr ligand, PCN, strongly induced expression of Cyp3a protein, moderately induced Cyp2c protein, but failed to induce Cyp1a, Cyp2b, or Cyp4a protein (Fig. 2*B*). RIF, which acts as a ligand for murine Pxr at the dose studied (60 mg/kg (34)), like PCN, induced Cyp3a and Cyp2c, but also induced Cyp4a. As with PCN, RIF failed to induce Cyp1a and Cyp2b. The Car activator, TCPOBOP, strongly induced Cyp2b, Cyp2c, and Cyp3a protein, weakly induced Cyp1a and Cyp4a, and weakly repressed Cyp2e expression. When TCPOBOP was combined with the Ahr ligand, TCDD, the TCPOBOP-type response was maintained, with additional strong induction of Cyp1a and Cyp4a. The alternative Car/Ahr activator combination, PB/βNF, induced a similar response, but without the suppression of Cyp2e. Addition of PCN to this combination increased the level of Cyp3a induction. With all combinations, cytosolic Gsta and Gstm enzymes were induced (Fig. 2*B*). As assessed by Western blotting, therefore, the combination of PCN, PB, and βNF provided a balanced enhancement of DME expression. This combination was selected for stimulation of metabolically labeled mice.

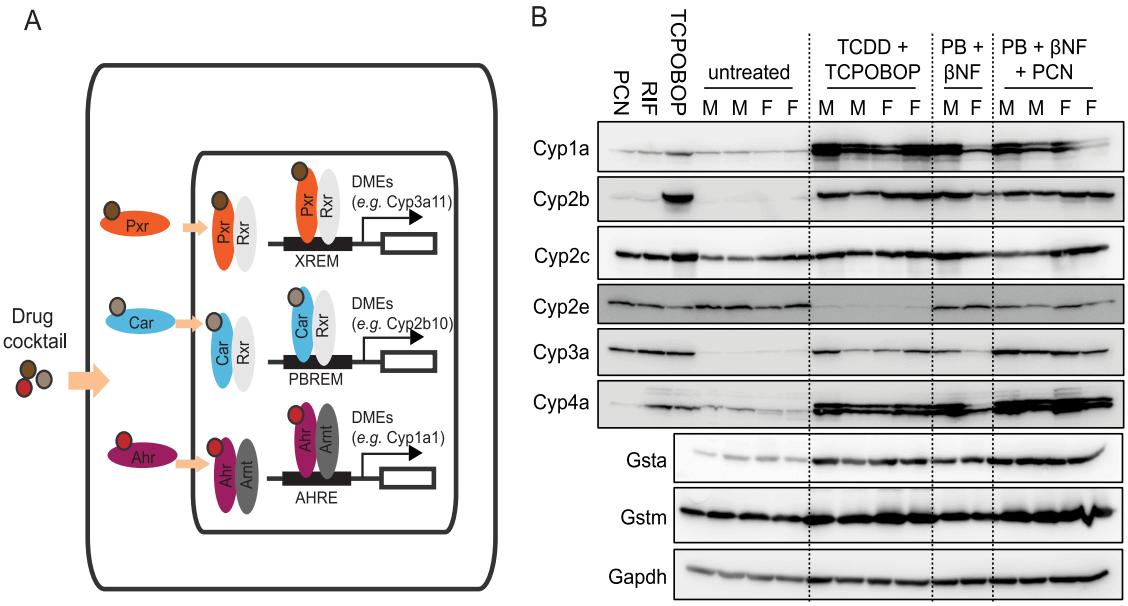

FIG. 2. **Enhancing protein expression in drug metabolism pathways by inducer mixture dosing.** *A*, Upon binding of ligand in cytosol, receptors translocate to the nucleus and form heterodimers with Rxr (Pxr and Car) or Arnt (Ahr). The induction of transcription of downstream genes is mediated by the binding of dimers to their specific promoter regions, for example, Pxr/Rxr binds in the promoter of Cyp3a11, Car/Rxr binds with Cyp2b10 and Ahr/Arnt binds with Cyp1a1. XREM, xenobiotic-responsive enhancer module; PBREM, phenobarbital-responsive enhancer module; AHRE, aryl hydrocarbon response element. *B*, Western blots of Cyp and Gst proteins in livers from male mice dosed with the Pxr/Car inducing agents, PCN, RIF, or TCPOBOP alone, or from male (M) and female (F) mice dosed with combinations of inducing agents, as detailed under "Experimental Procedures."

Characterization of Mixture-Dosed In Vivo SILAC Mice—Metabolically labeled mice were dosed with a mixture of PCN, PB, and βNF, as detailed under "Experimental Procedures." The liver proteome of one such "DME-enhanced" SILAC model was compared with that of age- and sex-matched unstimulated mice (10-band SDS-PAGE fractionation followed by in-gel digestion). Qualitatively by database search, a shift of protein identification (FDR = 0.1%) was observed with DME-enhanced SILAC mice gaining the detection of 593 protein groups, while losing 564 protein groups detectable in untreated mice (Fig. 3*A*). The total number of unique Cyp-derived peptides detected more than doubled, with an increase from 56 in the untreated mice to 115 in the mixture-dosed mice (Fig. 3*A*). For Cyp proteins identified by two or more unique peptides, the enhanced model showed increases in peptide number for enzymes including 1a1, 1a2, 2a4/2a5, 2a12, 2b10, 2c29, 2c54, 2j5, 3a11, 3a13, 17a1, and 51a1 (Fig. 3*B*). Decreases were observed for 2b9, 2c37, 2c44, 2d10, and 2e1. The expression of other DME superfamilies was not as profoundly affected (see data submitted to PRIDE).

To test the utility of this SILAC material in a proof-of-principle study, we investigated the potency of two compounds known to stimulate Cyp2b10 expression to varying degrees, TCPOBOP and EQ (35). Signal derived from the Cyp2b10 unique peptide, NLQELLDYIGHSVEK, was observed on stimulation of unlabeled "light" mice with both TCPOBOP (Fig. 3*D* and 3*G*) and EQ (Fig. 3*E* and *H*), but not in control animals (Fig. 3*C* and 3*F*). With a nonstimulated "heavy" liver sample acting as internal standard, the comparison of stimulation potency between these two compounds is not possible because of the lack of reference signal (Fig. 3*C*, 3*D*, and 3*E*). With Pxr/Car/Ahr-activator-stimulated "heavy" liver sample as internal standard, the induction of Cyp2b10 by TCPOBOP and EQ could be compared (Fig. 3*F*, 3*G*, and 3*H*). We found that TCPOBOP was ~4 times more potent than EQ in the induction of Cyp2b10, consistent with previous observations at the mRNA level (36).

Filtering Reliable Peptides for Quantification of DME by tHR/SIM—We have previously described the tHR/SIM workflow for identifying and characterizing peptides within mouse liver lysate (25). With the DME-enhanced SILAC materials, we adopted the same approach and employed a series of measures to retain only those peptides with high identification confidence scores and good analytical characteristics. DME-enhanced liver lysate was separated by SDS-PAGE in duplicate and two bands spanning defined molecular weight ranges – band 1: 80–40 kDa, band 2: 40–0 kDa – were excised for analysis by LC-MS/MS. Raw data were submitted to PEAKS software for protein identification (see supplemental Tables S6–S9 and supplemental Files S5 and S6). "Proteins.csv" and "protein-peptides.csv" output files for each defined molecular weight band (supplemental Tables S6–S9) were merged and appropriate −10LogP values applied to introduce a peptide FDR of 0.1% (band 1: 20.9, band 2: 22.9). Flanking amino acids were removed from the peptide sequences and peptides (1) without lysine, (2) that were not

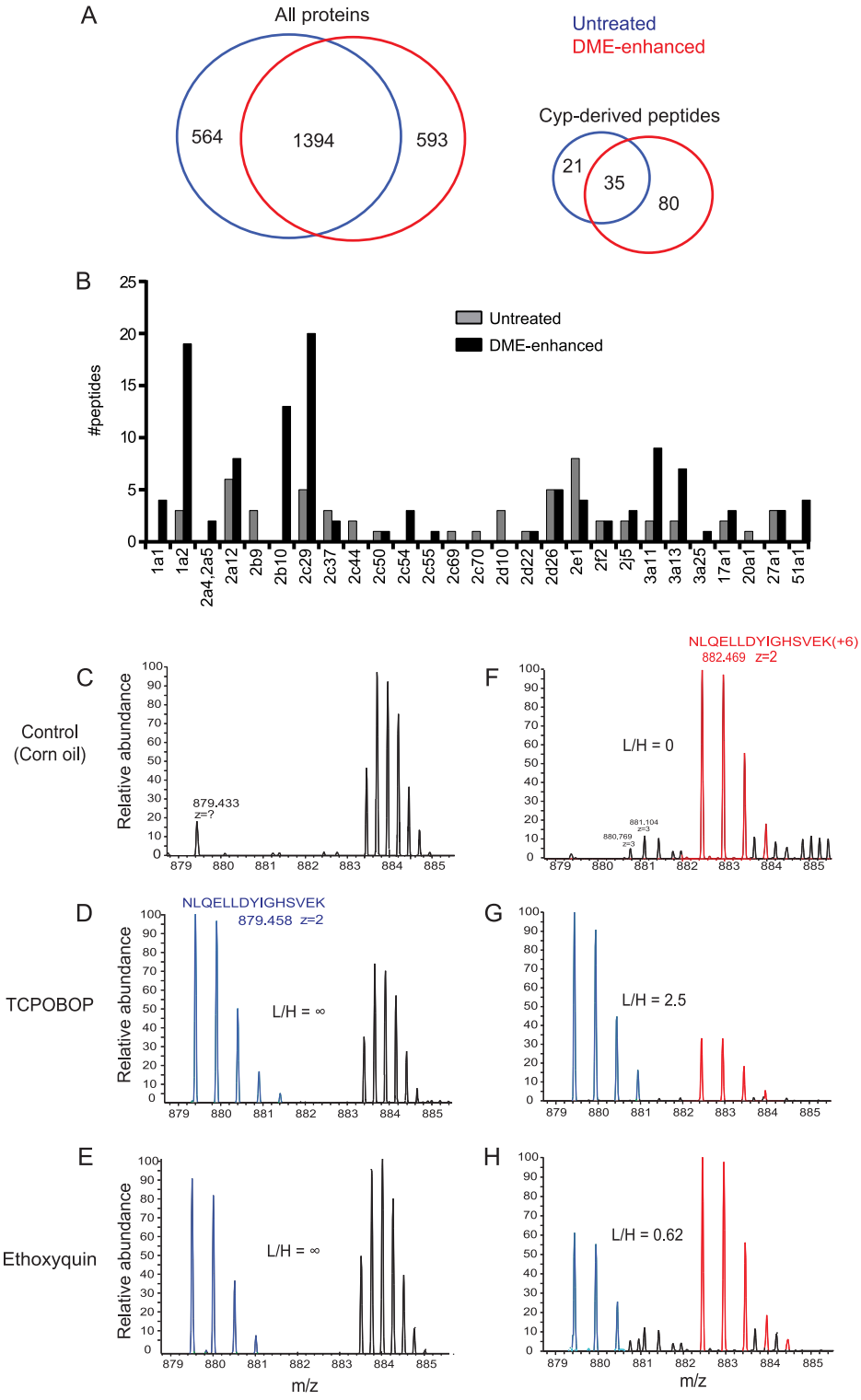

FIG. 3. **Liver proteome of the DME-enhanced *in vivo* SILAC mouse and its use in quantifying Cyp2b10 induction.** *A*, Comparison of the total number of proteins and the number of unique, lysine-containing Cyp-derived peptides identified in the liver proteome of untreated and DME-enhanced *in vivo* SILAC mice. Further details can be found in supplemental Tables S2–S5 and supplemental Files S3 and S4. *B*, Comparison of Cyp-derived unique peptides in the liver proteome of untreated and DME-enhanced *in vivo* SILAC mice. *C*, Measurement of the light and heavy species of the Cyp2b10-derived peptide, NLQELLDYIGHSVEK, by conventional SILAC with untreated unlabeled mice, *D*, TCPOBOP-dosed unlabeled mice and *E*, EQ-dosed unlabeled mice. *F*, The same peptide measured by DME-enhanced SILAC with untreated unlabeled mice, *G*, TCPOBOP-dosed unlabeled mice and *H*, EQ-dosed unlabeled mice.

unique, (3) from duplicate entries, and (4) from proteins that were outside the molecular weight range being targeted were discarded. A duplicate peptide list was then created containing the corresponding unlabeled version of each peptide, with *m/z* adjusted appropriately, and the labeled and unlabeled lists were merged. Appended to each list was an identically curated group of nonunique peptides. Typically, these were from two highly homologous proteins (such as Cyp2a4/2a5 or Akr1c12/1c13), although some were present in more than two proteins (for example Ugt2b5/2b17/2b38). The list for each

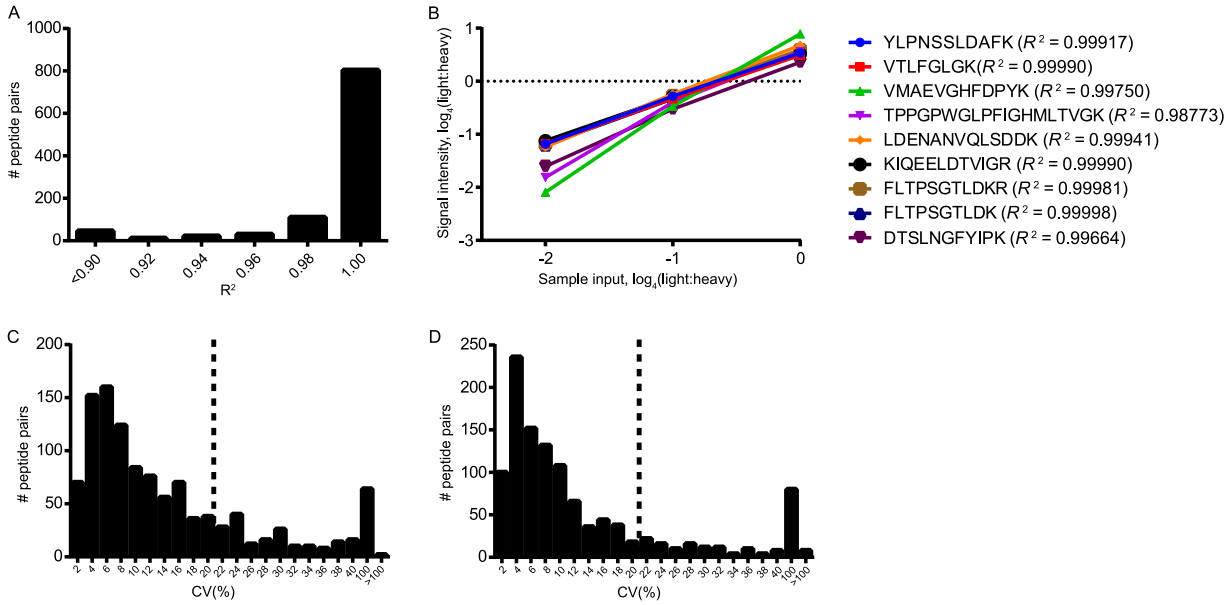

FIG. 4. **Filtering peptides showing high analytical performance.** *A*, Linearity (R^2 distribution) of calculated light to heavy ratios of SILAC peptide pairs across the 1:1, 1:0.25, and 1:0.0625 sample input range. 489 of 571 (86%) were ≥ 0.9. *B*, Linearity of peptides from Cyp1a1. All peptide R^2 values were ≥ 0.9. *C*, Intra-day variability of all peptide pairs. Pairs with CV ≤ 20% were retained; 433 of 571 (76%). *D*, Inter-day variability of all peptide pairs. Pairs with CV ≤ 20% were retained; 465 of 571 (81%).

molecular weight range was converted to a SIEVE-compatible seed file format with a retention time window of ± 3 min and the real (labeled) and theoretical (unlabeled) *m/z* ratios.

The analytical performance of SILAC peptide pairs was stress-tested in two ways. First, DME-enhanced labeled liver lysate was combined in three ratios (1:1, 1:0.25, and 1:0.0625) with pooled ($n = 2$) unlabeled liver lysate from age-, sex-, and drug dose-matched mice, in duplicate. Raw MS data were analyzed in SIEVE and, after a baseline correction step (as described under "Experimental Procedures"), average intensity values used to calculate ratios of light to heavy signal intensity for each peptide. The average ratio of technical replicates was then log4-transformed to evenly distribute the three data points, allowing calculation of an equally weighted R^2 value. Only peptide pairs with linearity $R^2 > 0.9$ (where the distribution of ratios of output intensity closely matched those of sample input and was sufficiently unperturbed by any background or contaminating signal) were retained (Fig. 4*A*). An example for peptides unique to Cyp1a1 is shown in Fig. 4*B*, where all nine met this criterion. Further examples for Cyp1a2, Cyp2b10, and Cyp2c29 are shown in supplemental Fig. S1. Secondly, DME-enhanced labeled liver lysate was combined 1:1 with the same pooled unlabeled liver lysate and analyzed in triplicate on three consecutive days. Peptide pairs that did not exhibit intra- (Fig. 4*C*) and/or inter-day (Fig. 4*D*) variability (CV) ≤20% were removed from the seed file. SIEVE output data along with linearity and precision calculations are provided as supplemental Tables S10 and S11). A summary of the number of peptides identified, containing lysine, and remaining after filtration is provided in Table I. The labeling efficiency of these peptides in the DME-enhanced liver sample was, on average, 98% (supplemental Fig. S2). The final seed files, filtered by R^2 and CV, are provided as supplemental Tables S12 and S13.

Characterization of the HRN Mouse Line by DME-Enhanced In Vivo SILAC—Developed in our laboratory, the HRN mouse line carries a liver-specific conditional deletion of cytochrome P450 reductase (*Por*), the primary electron donor for Cyp (26). The resulting near-ablation of hepatic P450 activity renders this model of utility in studies of the role of Cyp-mediated metabolism in defining drug disposition. Early characterization efforts revealed an increase in serum alanine aminotransferase, along with decreases in circulating cholesterol and triglycerides in the HRN line (26). The liver presented with hepatomegaly and impaired bile acid production, leading to cholesterol accumulation and hyperlipidemia. In addition, a fivefold increase in total P450 protein was observed, with induction of Cyp belonging to the 1a, 2b, 2c, 3a, and 4a subfamilies demonstrated by Western blot (37). This fivefold increase was not reflected by a concomitant increase in mRNA levels, which remained unchanged (38). Microarray and RT-PCR analyses detected up-regulation of the 2a4, 2c29, 3a11, 3a16, 4a10, 4a41, 7a1, 8b1, and 26a1 isoforms between 1.5 and 3.7-fold, with induction of Cyp2b10 by more than thirty-fold (38). Cyp2c70, 2d26, 2f2, 4v3, and 7b1 were down-regulated by 30–50%. For non-Cyp DME, Aldh1a7, and 3a2, and Gstm2 and m3 were up-regulated, whereas Hsd3b2, 3b5, and 11b1, and Gsta4 were down-regulated (38). In the present study, we used liver lysate from the DME-enhanced

TABLE I

Summary of filtering processes for the selection of seed peptide pairs. Of the 6348 peptides initially identified by PEAKS, 3856 of these contained lysine. 571 of these peptides were derived from DME and control proteins of interest. 386 peptides ultimately met all of the required criteria for DME quantification by tHR/SIM

	2 fraction PEAKS analysis (#peptides)		Seed files (#peptide pairs)	
	Identified, FDR = 0.1%	Contain K	First seed file	Second seed file (filtered for R^2 and CV)
Band 1	3306 (-10logP = 20.9)	1979	417	287
Band 2	3042 (-10logP = 22.9)	1877	154	99
Total	6348	3856	571	386

SILAC mouse to quantify protein-level changes in DME expression in the HRN line.

Liver samples from three male HRN mice and three age/sex-matched wild-type mice were analyzed (supplemental Table S14). Using the tHR/SIM-*in vivo* SILAC workflow, with a 3 min retention time window during data analysis, we confirmed that Por protein was deleted (Fig. 5*A*). Interestingly, we also observed an increase in expression of the alternative electron donor cytochrome b5, although this was not statistically significant (Fig. 5*A*). We observed significant induction of Cyp2b10 (16.8-fold), Cyp2b10/2b23 (7.1-fold), Cyp2c29 (6.6-fold), Cyp2c37 (2.8-fold), Cyp2c54 (2.7-fold), Cyp2c55 (20.0-fold), Cyp2c55/2g1(17.1-fold), Cyp2e1 (4.4-fold), Cyp3a11 (8.2-fold), Cyp3a11/44 (4.7-fold), and Cyp3a13 (2.8-fold) (Fig. 5*A*). These results are in full agreement with, and provide an increased level of detail to, the previous studies (26, 38). The only other Phase I enzyme to show statistically significant increase was Ces2a (2.4-fold), whereas there was a decrease in expression of Hsd11b1 (0.4-fold) and Hsd17b6 (0.3-fold) (Fig. 5*B*). For Phase II, Gstm2 (3.1-fold) and Gstm3 (18.1-fold) were up-regulated (Fig. 5*C*).

To provide additional confidence that the tHR/SIM approach was reliable, we extracted data for eight proteins, expression of which was considered unlikely to change significantly following *Por* deletion; β-actin-like protein 2 (Actbl2), actin-related protein 3 (Actr3), serum albumin (Alb), calreticulin (Calr), glyceraldehyde-3-phosphate dehydrogenase (Gapdh), tubulin α-4a, (Tuba4a), tubulin β-2a (Tubb2a), and tubulin β-4b (Tubb4b). There were marginal changes, most notably an increase in Calr, but none of these were statistically significant (supplemental Fig. S3).

DISCUSSION

Spike-in SILAC, in which tissue from a single metabolically labeled mouse can be used as an internal standard in multiple experiments (39), permits large-scale analysis of the proteome without the expensive requirement for maintenance of a labeled mouse colony. Relative quantification of proteins of interest can only be achieved, however, when those proteins are expressed at a detectable level in this animal. We have sought here to create a generic *in vivo* SILAC material suitable for quantification of as many DME, both basally expressed and requiring induction, as possible. Following simultaneous activation of Pxr, Car, and Ahr, we observed the widespread up-regulation of multiple Cyp, with an increase from 56 unique Cyp-derived peptides in untreated mice to 115 unique peptides following mixture-dosing (Fig. 3*A*). Crucially, the greatest induction was seen in the "xenobiotic-metabolizing" Cyps of the 1a, 2b, 2c, and 3a subfamilies (Fig. 3*A*), as opposed to those superfamily members with minor roles in this process (8, 40). Thus, synchronous nuclear receptor activation was demonstrated to be an appropriate means of enhancing the expression of DME-derived peptides in metabolically labeled liver for spike-in SILAC experiments.

The functional role and the transcriptional regulation of the CYP/Cyp 1A/a, 2B/b, 2C/c, 2D/d, and 3A/a xenobiotic metabolizing subfamilies are highly conserved between mice and men (8, 40). Mice from which these gene clusters have been knocked out and, in some cases, the orthologous human gene knocked in, have been in existence for a number of years (41). More recently, the simultaneous knockout/humanization of multiple clusters, along with that of their nuclear receptor regulators, has brought the prospect of effective *in vivo* preclinical modeling of PK/PD relationships closer to realization (42, 43). In order to maximize the utility of these models, a full understanding of their metabolic capacity is essential. We envisage that this DME-enhanced *in vivo* SILAC material will be of use in the characterization of these animals, both in their basal state and under chemical or pathological challenge. Moreover, it will support more complete preclinical evaluation of the PK, PD, and drug–drug interaction characteristics of candidate therapeutic compounds in these and other models.

In characterization of the HRN mouse line using the tHR/SIM workflow, we have demonstrated here that DME-enhanced SILAC material permits proteomic quantification at a level of detail unobtainable through Western blotting or conventional *in vivo* SILAC, on a scale impractical for AQUA. In agreement with mRNA analyses (38), we observed induction of multiple Cyp, Gstm, and repression of Hsd (Fig. 5), reinforcing the observation made in the previous study that ablation of Cyp function alters the balance of multiple metabolic pathways. Two notable contrasts with the microarray data should be emphasized. Firstly, although undetectable at the

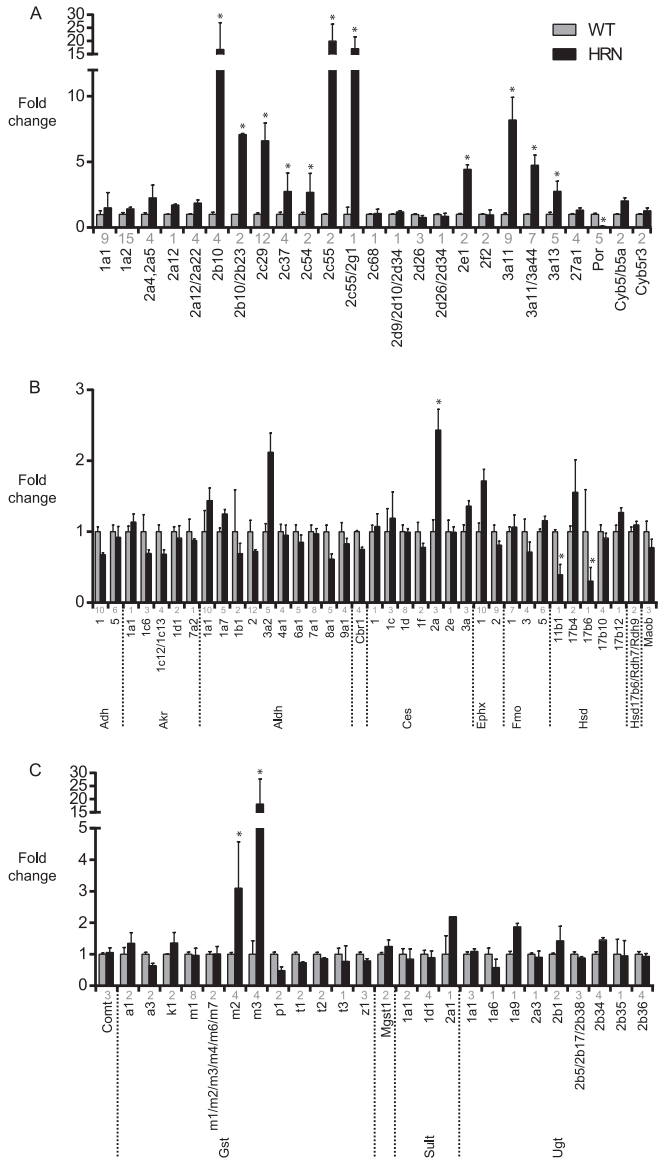

FIG. 5. **DME-enhanced tHR/SIM *in vivo* SILAC analysis of compensatory changes in the HRN mouse line.** *A*, Cyp and associated proteins, *B*, additional Phase I and *C*, Phase II enzymes were quantified. Gray bars: wild-type, black bars: HRN. Text in gray refers to the number of unique peptide pairs used for quantification. Data are presented as average fold change ± S.D. from three mice within each group with the following exceptions; Cyp2b0, Cyp2c55, and Cyp2c55/2g1, for which values were only quantifiable in two of three wild-type mice, Cyp2b10/2b23, for which values were only quantifiable in one wild-type and two HRN mice, and Sult2a1, for which values were only quantifiable in two wild-type and one HRN mouse.

mRNA level (38), we were able to demonstrate that Cyp1a1 protein levels remained unchanged (*i.e.* were low and not induced) following deletion of *Por* (Fig. 5*A*). Second, although Cyp2e1 mRNA levels were not altered (38), we identified statistically significant 4.4-fold induction of this enzyme at the protein level (Fig. 5*A*), indicative of a hitherto uncharacterized post-translational regulatory event. Taken together, our results are suggestive of Pxr/Car activation following *Por* deletion, as many of the target DME for these receptors are induced (6, 44). This conclusion supports the findings of Finn *et al.*, where accumulation of unsaturated fatty acids in the HRN liver was shown to activate Car and, to a lesser extent, Pxr (45). We are currently testing the application of DME-enhanced SILAC in facilitating the full characterization of complex humanized mouse models.

DME-enhanced SILAC offers two main advantages; it enables quantification of DME that are normally expressed at very low levels, and it improves confidence in quantification of those DME that are basally quantifiable, but also subject to induction, by increasing the number of peptides measured. The latter effect is important for reliable protein quantification because an amino acid substitution (by, for example, mutation) or a post-translational modification can affect the m/z ratio of a tryptic peptide and thereby influence quantification results. Inclusion of a greater number of targeted peptides through DME-enhanced SILAC could mitigate this potentially critical yet unpredictable effect, rendering it less problematic than with other proteomic strategies where only one or two peptides per protein are monitored.

Although gains were made with DME-enhancement in the pathways targeted by the inducer compounds, Cyp 2b9, 2c44, 2c69, 2c70, 2d10, and 20a1 were not detected in the initial characterization experiment (Fig. 3*B*). This may be indicative of down-regulation of their expression because of a diversion of cellular resource from endogenous to exogenous metabolism (for example, cyp2c44 is involved in eicosanoid metabolism (46)). Should quantification of these enzymes be required, however, one solution would be to combine both unstimulated and DME-enhanced labeled liver lysates for use as the internal standard. As the expression of "suppressed" proteins tends to be low in inducer-naïve liver (as evidenced by the small number of peptides detected (Fig. 3*B*)), however, we would not anticipate a substantial improvement in their detection without severe decreases in signal from the induced enzymes. An alternative solution would be to append light peptide-specific information for the lost signals to the seed files, then to calculate their intensities relative to miscellaneous heavy peptides with similar properties.

We have utilized the tHR/SIM workflow described previously to demonstrate the application of DME-enhanced SILAC, as the downstream data analysis can be significantly simplified. Alternative data analysis software, such as MaxQuant (47) or Skyline (48), could be used instead. It is also theoretically possible to apply SWATH (49), or parallel reaction monitoring (50) workflows, with quantification based on MS1 or MS2 signals. In addition, the use of newer, more advanced instrumentation will also significantly improve the number of proteins quantifiable using any of these workflows. Many of the proteins known to be regulated by Pxr, Car, and Ahr have not been detected in the present study, implying that the benefits of DME-enhancement would be recapitulated

with a different subset of these target proteins at greater analytical sensitivity.

In succession to the tHR/SIM seed peptide filtering workflow reported previously (25), here we have adapted a more stringent selection process, following principles from the bioanalytical validation procedure (51). We included intra- and inter-day variability and dilution linearity tests to filter out the peptides with poor analytical performance in the initial targeted seed list. Approximately one third (185 of 571) of the original seed peptides were excluded during this process, therefore the majority of sources of imprecision that may otherwise have contributed to variability in the data were eliminated. Additional potential sources of variability that remain include low (and thus variable) target signals (as seen with Cyp2b10 in the HRN analysis), imprecision in gel-cutting, and artifact/contaminant signals. Nonetheless, we believe the filtering process applied here is necessary and sufficient to ensure data quality.

In summary, we have designed, implemented and validated a proteomic strategy for quantification of 386 SILAC peptide pairs, representing 98 DMEs from all major superfamilies, in mouse liver. Crucially, through the simultaneous activation of the three most physiologically important regulators of DME expression, Pxr, Car, and Ahr, in metabolically labeled mice, we have enabled quantification of enzymes that are maintained at a very low basal level of expression and would otherwise have been undetectable, while increasing the number of peptides available for quantification of inducible enzymes that are detectable at the basal level. This pathway enhancement facilitates a holistic appraisal of metabolic potential at the protein level in a generic context and will be of utility in identifying and understanding the changes that occur in preclinical models of drug disposition.

Acknowledgments—We thank Mrs. Julia Carr for assistance with animal work and Professor John Hayes for anti-Gst antibodies.

* This study was supported by Cancer Research UK, program grant C4639/A12330. PF was supported by National Children's Research Centre and Science Foundation Ireland. The mass spectrometry proteomics data have been deposited to the ProteomeXchange Consortium (52) via the PRIDE partner repository with the dataset identifier PXD001210. Please see Supplemental Information for a description of the files deposited.

[S] This article contains supplemental Figs. S1 to S3, Tables S1 to S14, and Files S1 to S6.

¶ To whom correspondence should be addressed: Jacqui Wood Cancer Centre, Medical Research Institute, Ninewells Hospital and Medical School, University of Dundee, Dundee, DD1 9SY, Scotland. Tel.: +44 (0)1382 386901; E-mail: j.t.j.huang@dundee.ac.uk.

REFERENCES

1. Wienkers, L. C., and Heath, T. G. (2005) Predicting *in vivo* drug interactions from *in vitro* drug discovery data. *Nat. Rev. Drug Discov.* **4,** 825–833
2. http://www.fda.gov/downloads/Drugs/GuidanceComplianceRegulatoryInformation/Guidances/ucm292362.pdf
3. http://www.ema.europa.eu/docs/en_GB/document_library/Scientific_guideline/2012/07/WC500129606.pdf
4. Xu, C., Li, C. Y., and Kong, A. N. (2005) Induction of phase I, II, and III drug metabolism/transport by xenobiotics. *Arch. Pharm. Res.* **28,** 249–268
5. Tolson, A. H., and Wang, H. (2010) Regulation of drug-metabolizing enzymes by xenobiotic receptors: PXR and CAR. *Adv. Drug Deliv. Rev.* **62,** 1238–1249
6. Maglich, J. M., Stoltz, C. M., Goodwin, B., Hawkins-Brown, D., Moore, J. T., and Kliewer, S. A. (2002) Nuclear pregnane x receptor and constitutive androstane receptor regulate overlapping but distinct sets of genes involved in xenobiotic detoxification. *Mol. Pharmacol.* **62,** 638–646
7. Willson, T. M., and Kliewer, S. A. (2002) PXR, CAR, and drug metabolism. *Nat. Rev. Drug Discov.* **1,** 259–266
8. Hrycay, E. G., and Bandiera, S. M. (2009) Expression, function, and regulation of mouse cytochrome P450 enzymes: comparison with human P450 enzymes. *Curr. Drug Metab.* **10,** 1151–1183
9. Streetman, D. S., Bertino, J. S., Jr., and Nafziger, A. N. (2000) Phenotyping of drug-metabolizing enzymes in adults: a review of in-vivo cytochrome P450 phenotyping probes. *Pharmacogenetics* **10**, 187–216
10. Court, M. H. (2005) Isoform-selective probe substrates for *in vitro* studies of human UDP-glucuronosyltransferases. *Methods Enzymol.* **400,** 104–116
11. Evans, W. E., and Relling, M. V. (1999) Pharmacogenomics: translating functional genomics into rational therapeutics. *Science* **286,** 487–491
12. Ohtsuki, S., Schaefer, O., Kawakami, H., Inoue, T., Liehner, S., Saito, A., Ishiguro, N., Kishimoto, W., Ludwig-Schwellinger, E., Ebner, T., and Terasaki, T. (2011) Simultaneous absolute protein quantification of transporters, cytochromes P450, and UDP-glucuronosyltransferases as a novel approach for the characterization of individual human liver: comparison with mRNA levels and activities. *Drug Metab. Dispos.* **40,** 83–92
13. Michaels, S., and Wang, M. Z. (2014) The revised human liver cytochrome P450 "pie": absolute protein quantification of CYP4F and CYP3A enzymes using targeted quantitative proteomics. *Drug Metab. Dispos.* **42,** 1241–1251
14. Hersman, E. M., and Bumpus, N. N. (2014) A targeted proteomics approach for profiling murine cytochrome P450 expression. *J. Pharmacol. Exp. Ther.* **349,** 221–228
15. Achour, B., Russell, M. R., Barber, J., and Rostami-Hodjegan, A. (2014) Simultaneous quantification of the abundance of several cytochrome P450 and uridine 5′-diphospho-glucuronosyltransferase enzymes in human liver microsomes using multiplexed targeted proteomics. *Drug Metab, Dispos.* **42,** 500–510
16. Shrivas, K., Mindaye, S. T., Getie-Kebtie, M., and Alterman, M. A. (2013) Mass spectrometry-based proteomic analysis of human liver cytochrome(s) P450. *Toxicol. Appl. Pharmacol.* **267,** 125–136
17. Karlsen, O. A., Puntervoll, P., and Goksoyr, A. (2012) Mass spectrometric analyses of microsomal cytochrome P450 isozymes isolated from beta-naphthoflavone-treated Atlantic cod (Gadus morhua) liver reveal insights into the cod CYPome. *Aquat. Toxicol.* **108,** 2–10
18. Williamson, B. L., Purkayastha, S., Hunter, C. L., Nuwaysir, L., Hill, J., and Easterwood, L. (2010) Quantitative protein determination for CYP induction via LC-MS/MS. *Proteomics* **11,** 33–41
19. Qiu, X., Zhang, H., and Lai, Y. (2014) Quantitative targeted proteomics for membrane transporter proteins: method and application. *AAPS J.* **16,** 714–726
20. Jani, M., Ambrus, C., Magnan, R., Jakab, K. T., Beery, E., Zolnerciks, J. K., and Krajcsi, P. (2014) Structure and function of BCRP, a broad specificity transporter of xenobiotics and endobiotics. *Arch. Toxicol.* **88,** 1205–1248
21. Groer, C., Bruck, S., Lai, Y., Paulick, A., Busemann, A., Heidecke, C. D., Siegmund, W., and Oswald, S. (2013) LC-MS/MS-based quantification of clinically relevant intestinal uptake and efflux transporter proteins. *J. Pharm. Biomed. Anal.* **85,** 253–261
22. Sakamoto, A., Matsumaru, T., Yamamura, N., Uchida, Y., Tachikawa, M., Ohtsuki, S., and Terasaki, T. (2013) Quantitative expression of human drug transporter proteins in lung tissues: analysis of regional, gender, and interindividual differences by liquid chromatography-tandem mass spectrometry. *J. Pharm. Sci.* **102,** 3395–3406
23. Gerber, S. A., Rush, J., Stemman, O., Kirschner, M. W., and Gygi, S. P. (2003) Absolute quantification of proteins and phosphoproteins from cell lysates by tandem MS. *Proc. Natl. Acad. Sci. U.S.A.* **100,** 6940–6945
24. Liebler, D. C., and Ham, A. J. (2009) Spin filter-based sample preparation for shotgun proteomics. *Nat. Methods* **6,** 785–786
25. Macleod, A. K., Zang, T., Riches, Z., Henderson, C. J., Wolf, C. R., and Huang, J. T. (2014) A targeted *in vivo* SILAC approach for quantification of drug metabolism enzymes: regulation by the constitutive androstane

receptor. *J. Proteome Res.* **13,** 866–874
26. Henderson, C. J., Otto, D. M., Carrie, D., Magnuson, M. A., McLaren, A. W., Rosewell, I., and Wolf, C. R. (2003) Inactivation of the hepatic cytochrome P450 system by conditional deletion of hepatic cytochrome P450 reductase. *J. Biol. Chem.* **278,** 13480–13486
27. Kruger, M., Moser, M., Ussar, S., Thievessen, I., Luber, C. A., Forner, F., Schmidt, S., Zanivan, S., Fassler, R., and Mann, M. (2008) SILAC mouse for quantitative proteomics uncovers kindlin-3 as an essential factor for red blood cell function. *Cell* **134,** 353–364
28. Shevchenko, A., Tomas, H., Havlis, J., Olsen, J. V., and Mann, M. (2006) In-gel digestion for mass spectrometric characterization of proteins and proteomes. *Nat. Protoc.* **1,** 2856–2860
29. Meehan, R. R., Forrester, L. M., Stevenson, K., Hastie, N. D., Buchmann, A., Kunz, H. W., and Wolf, C. R. (1988) Regulation of phenobarbital-inducible cytochrome P-450s in rat and mouse liver following dexamethasone administration and hypophysectomy. *Biochem. J.* **254,** 789–797
30. Forrester, L. M., Henderson, C. J., Glancey, M. J., Back, D. J., Park, B. K., Ball, S. E., Kitteringham, N. R., McLaren, A. W., Miles, J. S., Skett, P., and et al (1992) Relative expression of cytochrome P450 isoenzymes in human liver and association with the metabolism of drugs and xenobiotics. *Biochem. J.* **281,** 359–368
31. Finn, R. D., McLaughlin, L. A., Ronseaux, S., Rosewell, I., Houston, J. B., Henderson, C. J., and Wolf, C. R. (2008) Defining the *in vivo* role for cytochrome b5 in cytochrome P450 function through the conditional hepatic deletion of microsomal cytochrome b5. *J. Biol. Chem.* **283,** 31385–31393
32. McLellan, L. I., and Hayes, J. D. (1989) Differential induction of class alpha glutathione S-transferases in mouse liver by the anticarcinogenic antioxidant butylated hydroxyanisole. Purification and characterization of glutathione S-transferase Ya1Ya1. *Biochem. J.* **263,** 393–402
33. Olsen, J. V., de Godoy, L. M., Li, G., Macek, B., Mortensen, P., Pesch, R., Makarov, A., Lange, O., Horning, S., and Mann, M. (2005) Parts per million mass accuracy on an Orbitrap mass spectrometer via lock mass injection into a C-trap. *Mol. Cell. Proteomics* **4,** 2010–2021
34. Scheer, N., Ross, J., Rode, A., Zevnik, B., Niehaves, S., Faust, N., and Wolf, C. R. (2008) A novel panel of mouse models to evaluate the role of human pregnane X receptor and constitutive androstane receptor in drug response. *J. Clin. Invest.* **118,** 3228–3239
35. Cheng, X., Maher, J., Dieter, M. Z., and Klaassen, C. D. (2005) Regulation of mouse organic anion-transporting polypeptides (Oatps) in liver by prototypical microsomal enzyme inducers that activate distinct transcription factor pathways. *Drug Metab. Dispos.* **33,** 1276–1282
36. Ahn, M. J., Tsai, C. M., Hsia, T. C., Wright, E., Chang, J. W., Kim, H. T., Kim, J. H., Kang, J. H., Kim, S. W., Bae, E. J., Kang, M., Lister, J., and Walzer, S. Cost-effectiveness of bevacizumab-based therapy versus cisplatin plus pemetrexed for the first-line treatment of advanced nonsquamous NSCLC in Korea and Taiwan. *Asia Pac. J. Clin. Oncol.* **7,** 22–33
37. Chanas, S. A., Jiang, Q., McMahon, M., McWalter, G. K., McLellan, L. I., Elcombe, C. R., Henderson, C. J., Wolf, C. R., Moffat, G. J., Itoh, K., Yamamoto, M., and Hayes, J. D. (2002) Loss of the Nrf2 transcription factor causes a marked reduction in constitutive and inducible expression of the glutathione S-transferase Gsta1, Gsta2, Gstm1, Gstm2, Gstm3, and Gstm4 genes in the livers of male and female mice. *Biochem. J.* **365,** 405–416
38. Wang, X. J., Chamberlain, M., Vassieva, O., Henderson, C. J., and Wolf, C. R. (2005) Relationship between hepatic phenotype and changes in gene expression in cytochrome P450 reductase (POR) null mice. *Biochem. J.* **388,** 857–867
39. Geiger, T., Wisniewski, J. R., Cox, J., Zanivan, S., Kruger, M., Ishihama, Y., and Mann, M. (2011) Use of stable isotope labeling by amino acids in cell culture as a spike-in standard in quantitative proteomics. *Nat. Protoc* **6,** 147–157
40. Nelson, D. R., Zeldin, D. C., Hoffman, S. M., Maltais, L. J., Wain, H. M., and Nebert, D. W. (2004) Comparison of cytochrome P450 (CYP) genes from the mouse and human genomes, including nomenclature recommendations for genes, pseudogenes, and alternative-splice variants. *Pharmacogenetics* **14,** 1–18
41. Cheung, C., and Gonzalez, F. J. (2008) Humanized mouse lines and their application for prediction of human drug metabolism and toxicological risk assessment. *J. Pharmacol. Exp. Ther.* **327,** 288–299
42. Hasegawa, M., Kapelyukh, Y., Tahara, H., Seibler, J., Rode, A., Krueger, S., Lee, D. N., Wolf, C. R., and Scheer, N. (2011) Quantitative prediction of human pregnane X receptor and cytochrome P450 3A4 mediated drug–drug interaction in a novel multiple humanized mouse line. *Mol. Pharmacol.* **80,** 518–528
43. Scheer, N., McLaughlin, L. A., Rode, A., Macleod, A. K., Henderson, C. J., and Wolf, C. R. (2014) Deletion of 30 murine cytochrome p450 genes results in viable mice with compromised drug metabolism. *Drug Metab. Dispos.* **42,** 1022–1030
44. Tojima, H., Kakizaki, S., Yamazaki, Y., Takizawa, D., Horiguchi, N., Sato, K., and Mori, M. (2012) Ligand dependent hepatic gene expression profiles of nuclear receptors CAR and PXR. *Toxicol. Lett.* **212,** 288–297
45. Finn, R. D., Henderson, C. J., Scott, C. L., and Wolf, C. R. (2009) Unsaturated fatty acid regulation of cytochrome P450 expression via a CAR-dependent pathway. *Biochem. J.* **417,** 43–54
46. DeLozier, T. C., Tsao, C. C., Coulter, S. J., Foley, J., Bradbury, J. A., Zeldin, D. C., and Goldstein, J. A. (2004) CYP2C44, a new murine CYP2C that metabolizes arachidonic acid to unique stereospecific products. *J. Pharmacol. Exp. Ther.* **310,** 845–854
47. Cox, J., and Mann, M. (2008) MaxQuant enables high peptide identification rates, individualized p.p.b.-range mass accuracies and proteome-wide protein quantification. *Nat. Biotechnol.* **26,** 1367–1372
48. MacLean, B., Tomazela, D. M., Shulman, N., Chambers, M., Finney, G. L., Frewen, B., Kern, R., Tabb, D. L., Liebler, D. C., and MacCoss, M. J. (2010) Skyline: an open source document editor for creating and analyzing targeted proteomics experiments. *Bioinformatics* **26,** 966–968
49. Gillet, L. C., Navarro, P., Tate, S., Rost, H., Selevsek, N., Reiter, L., Bonner, R., and Aebersold, R. (2012) Targeted data extraction of the MS/MS spectra generated by data-independent acquisition: a new concept for consistent and accurate proteome analysis. *Mol. Cell. Proteomics* **11,** O111 016717
50. Gallien, S., Duriez, E., Crone, C., Kellmann, M., Moehring, T., and Domon, B. (2012) Targeted proteomic quantification on quadrupole-orbitrap mass spectrometer. *Mol. Cell. Proteomics* **11,** 1709–1723
51. http://www.fda.gov/downloads/AnimalVeterinary/GuidanceComplianceEnforcement/GuidanceforIndustry/ucm052379.pdf
52. Vizcaino, J. A., Deutsch, E. W., Wang, R., Csordas, A., Reisinger, F., Rios, D., Dianes, J. A., Sun, Z., Farrah, T., Bandeira, N., Binz, P. A., Xenarios, I., Eisenacher, M., Mayer, G., Gatto, L., Campos, A., Chalkley, R. J., Kraus, H. J., Albar, J. P., Martinez-Bartolome, S., Apweiler, R., Omenn, G. S., Martens, L., Jones, A. R., and Hermjakob, H. (2014) ProteomeXchange provides globally coordinated proteomics data submission and dissemination. *Nat. Biotechnol.* **32,** 223–226